

TECHNICAL UNIVERSITY OF CRETE
ELECTRICAL AND COMPUTER ENGINEERING SCHOOL
TELECOMMUNICATIONS DIVISION



City-wide Rooftop Networking

by

Panagiotis Oikonomakos

A THESIS SUBMITTED IN PARTIAL FULFILLMENT OF
THE REQUIREMENTS FOR THE MASTER OF

ELECTRICAL AND COMPUTER ENGINEERING

December 2017

THESIS COMMITTEE

Associate Professor Aggelos Bletsas, *Thesis Supervisor*

Associate Professor George N. Karystinos

Associate Professor Eftichios Koutroulis

Abstract

Mesh (802.11s) networks are inherently resource constrained, in terms of transmission power, as well as bandwidth. It is essential to formulate coloring schemes that explicitly protect sensitive links. This work offers a coloring algorithm that protects specific links from interference, using network planner-defined weights. The network consists of nodes that accommodate a variable number of 802.11s radio interfaces, with different kinds of *directive* antennas, targeting *city-wide* deployments. The proposed algorithm is applied to a carefully crafted conflict graph, with merged vertices that share common radio interfaces. Semidefinite programming (SDP) is used to approximate the chromatic number of the conflict graph. Evaluation is performed both in terms of simulation in modified NS3 (to accommodate multiple directive radio interfaces per node), as well as experimental results across a city-wide deployment; the greater area of Chania city is covered, spanning ranges in the order of 5.5 km. It is demonstrated that the proposed link protection methodology outperforms prior art that avoids protecting specific links; improvements are observed both in terms of average, as well as minimum (worst-case) throughput. Such quality-of-service (QoS) improvement is a key attribute in critical applications and may be deemed crucial in practical, city-wide, rooftop networking.

Acknowledgements

I would like to express my gratitude to Prof. Aggelos Bletsas for his guidance and support, for the implementation of this thesis. His extensive knowledge and experience have been important in achieving my goals. I would also like to thank all the group members i have collaborated with, for their significant contribution, especially Mr. Dimitris Ntilis and Dr. Panos N. Alevizos. Finally, I would like to thank my family and my friends for their support throughout the years of my studies. They have always been there for me and without them this thesis would have never been completed.

Table of Contents

Table of Contents	4
List of Figures	5
1 Introduction	7
2 System Model & Deployment	11
3 Conflict Graph Creation & Simplification	16
4 Conflict Graph Coloring	20
4.1 SDP for Graph Chromatic Number Estimation	20
4.2 Link Protection Coloring Algorithm (LPCA)	21
4.3 Frequency Channel Probing Algorithm (FCPA)	23
5 Results	26
5.1 Simulation Results	26
5.2 Experimental Results	34
6 Conclusion	36
 Appendices	
A Proof of Theorem 1	37
Bibliography	39

List of Figures

1.1	City-scale, mesh network topology, tested in this work (with connectivity in Fig. 2.1). Extended area must be served with limited resources (i.e., transmission power and bandwidth). Coloring in 802.11s must be performed judiciously.	7
2.1	Connectivity Graph of network nodes in Fig. 1.1; routing and interference links with solid and dashed lines, respectively. Multiple radio interfaces are depicted with rectangles or triangles, corresponding to narrow beamwidth and sector directional antennas, respectively.	11
2.2	Connectivity Graph of network nodes with External Interference.	11
2.3	ALIX 3D2 in a waterproof case with an antenna attached to a radio interface.	12
2.4	Deployment phase.	13
2.5	City-deployed node with multiple directive radio interfaces. . .	14
3.1	Initial Conflict Graph.	16
3.2	Conflict Graph before and after merging. Left graph above is equivalent to conflict graph of Fig. 3.1.	17
3.3	Initial Conflict Graph with External Interference.	17
3.4	Conflict Graph before and after merging with External Interference.	18
5.1	Extended Conflict Graph.	26
5.2	Average and Minimum Throughput of Source Nodes.	26
5.3	NS3 Topology of the network.	27
5.4	First Extended NS3 Topology.	28
5.5	Second Extended NS3 Topology.	29
5.6	Third Extended NS3 Topology.	30
5.7	Extended Conflict Graph with External Interference.	31
5.8	Average and Minimum Throughput Before Probing (LPCA without FCPA) and After Probing (LPCA with FCPA). . . .	31
5.9	NS3 Topology of the network with External Interference. . . .	32
5.10	First Extended NS3 Topology with External Interference. . . .	32

5.11	Second Extended NS3 Topology with External Interference.	. .	33
5.12	Third Extended NS3 Topology with External Interference.	. .	33

Chapter 1

Introduction

City-wide wireless mesh (802.11s) networks, targeting critical applications, oppose several challenges. Mesh nodes can only be installed at specific locations, limiting the potential number of wireless paths between any two nodes and thus, reducing diversity. Additionally, links in the order of 5-6 kilometers have to be implemented, with limited equivalent isotropic radiated power (EIRP) at each transmitter (e.g., not exceeding 20 dBm at the 2.4 GHz band). On top of that, 802.11 frequency bands in a city are crowded (as a result of being unlicensed), causing additional interference in the reception of various transmissions. Fig. 1.1 offers an example of a network where terminals have to be deployed at very specific locations, targeting water management [1], [2]. Despite the challenges, 802.11 links have been recently studied for medium-range [3] to extended-range [4] scenarios.



Figure 1.1: City-scale, mesh network topology, tested in this work (with connectivity in Fig. 2.1). Extended area must be served with limited resources (i.e., transmission power and bandwidth). Coloring in 802.11s must be performed judiciously.

Prior art in graph coloring (e.g., [5]) is quite rich and the discussion is limited in multi-radio 802.11s networks. A centralized and a distributed algorithm is offered in [6]. The centralized approach is based on the popular heuristic TABU search technique [7] that has been used in the past in graph coloring problems. The distributed approach is based on the greedy approximation algorithm for Max K-cut problem in graphs. This work considers a centralized approach and leaves the distributed approach for future work. Multiple radio interfaces with omni-directional antennas per node were used in [6]. In sharp contrast, this work considers variable number of radio interfaces with different kinds of directivity antennas (broad and narrow beamwidth) per node. The directivity of the multiple antennas at each node adds extra constraints that must be explicitly addressed by the coloring algorithm, so that in-network (internal) interference is reduced.

Minimum-color path problems that find paths satisfying various reliability objectives, such as minimizing the probability of failure on a path, are discussed in [8]. A routing algorithm is proposed in [9], using beamforming antennas. This work differs from [8] and [9] as the routing links are defined by the proactive routing mode of Hybrid Wireless Mesh Protocol (HWMP, the default 802.11s routing protocol). In the proactive mode of HWMP, one or more nodes are declared as gateways by the network manager and the routing protocol creates paths from each node of the network to the gateways [10], [11]. The airtime metric is used for the selection of the routing paths, which is the default metric of HWMP; such metric depends on various link-level parameters, including frame transmission rate and bit error rate. Additionally, in [9] the antenna model can operate in two modes, either omni-directional or directional. This greatly differs from this work, where multiple directional antennas were used without the ability to switch to omni-directional mode.

A joint optimization of topology, routing and frequency channel assignment algorithm is proposed in [12]. In this work, the network topology cannot be modified due to the limitations imposed by the landscape and the specific locations the nodes must be installed. On top of that, the large distance between the nodes does not allow any changes to the orientation of the antennas. Additionally, as mentioned earlier this work adds value and enhances the proactive mode of HWMP, by applying a frequency channel allocation policy, given the HWMP routing tree. Applications with other routing methods for rooftop networking [13], [14] are possible.

The allocation policies proposed in [15–18] focus on maximizing the overall network throughput. In sharp contrast, this work provides a frequency channel allocation policy which protects specific links of the network while possibly lowering average throughput as a trade-off. Nodes depending on

weaker links in resource constrained mesh networks, often encounter connectivity loss issues due to heavy interference. The latter frequency channel allocation policy mitigates this phenomenon.

Interference might be caused by the nodes of the network transmitting at the same frequency channel (internal), as well as from sources outside of the network (external). In this work, a coloring algorithm, called Link Protection Coloring Algorithm (LPCA), is proposed. LPCA is an extension of the coloring algorithm presented in [1], whose key feature is the protection of the more distant links from internal interference. This feature is further extended so that other weight definitions can be used. Additionally, the algorithm is improved for the case where remaining internal interference cannot be avoided.

In order to mitigate the external interference along with the internal interference, another algorithm is proposed, called Frequency Channel Probing Algorithm (FCPA). FCPA produces QoS statistics for the links of the network by scanning the available frequency channels. These statistics can be harnessed as input for LPCA in order to produce colorings that mitigate both the internal and the external interference.

The priority of each link is based on network planner-defined weights. Multiple weights are used, each one at a different stage of the algorithm's execution. This results in a better control of the applied frequency channel allocation policy, e.g. protecting the weaker links thus improving minimum throughput while possibly lowering average throughput as a trade-off.

The procedure of producing a coloring for the network starts with the connectivity graph which contains all the possible links of the network. Then, a routing tree is produced by the proactive mode of HWMP, using one or more nodes as gateways. The links of the connectivity graph that are excluded from the routing tree, are considered interference links. Then, the conflict graph creation algorithm proposed in [1] is employed. A vertex merging technique for the conflict graph of the network under study is then presented, exploiting the fact that some vertices in the conflict graph share common radio interfaces. The problem of determining the chromatic number $\chi(G)$ for graph G is NP-complete. Therefore, no polynomial algorithm is known for calculating $\chi(G)$. The relaxed semidefinite problem (SDP) proposed in [19] is used to approximate the chromatic number of the conflict graph. The dependencies of the vertices that share a common interface in the original conflict graph, cannot be expressed in the SDP; thus, the modified conflict graph is used. Finally, LPCA is executed at the modified conflict graph. LPCA can be executed with or without FCPA. For the case that LPCA is used without FCPA, only internal interference is mitigated by the produced coloring. If LPCA is used in conjunction with FCPA, external interference

is also detected and alleviated to a certain degree.

The contributions of this work are:

- A merging technique of the vertices that share a common interface in the conflict graph is proposed. In the merged conflict graph, SDP can be used to approximate the chromatic number of the conflict graph.
- An algorithm called LPCA is designed that mitigates internal interference giving priority to specific links. Its key feature is that it improves minimum throughput, preventing nodes depending on weaker links from being completely cut off from the rest of the network due to heavy internal interference.
- A supplementary algorithm of LPCA is developed, called FCPA that scans the available frequency channels, producing QoS statistics for each link used by LPCA, in order to protect the links from external along with the internal interference.
- A modification of NS3 is offered in order to accommodate the use of multiple interfaces per node, with directional antennas in 802.11s mesh networks using HWMP.

Throughput performance of LPCA and FCPA is studied and compared with state-of-the-art, including average as well as worst-case, minimum throughput; the latter is a key QoS attribute in critical applications, as for city-wide water management.

The rest of the work is organized as follows. Chapter 2 offers the basic assumptions and notation of the system model and presents the deployment of the network. Chapter 3 describes the simplified conflict graph (after merging specific vertices) in which coloring will be performed. Chapter 4 presents LPCA and FCPA (and for completeness, a prior art method for chromatic number estimation). Chapter 5 offers the simulation and experimental results of the network under study and discusses QoS findings. Finally, work is concluded in Chapter 6.

Chapter 2

System Model & Deployment

The connectivity graph $G(V, E)$ of the network is shown in Fig. 2.1. Each $v \in V$ corresponds to a radio interface and each $e \in E$ corresponds to a link between two radio interfaces. The routing links of the network $G_r(V, E_r)$, where $E_r \subseteq E$, are represented with solid lines. The interference links $E \setminus E_r$ are represented with dashed lines. To refer to the radio interfaces of a node, e.g., radio interface 3 of node 1, the following notation is used: $N_1 : r_3$.

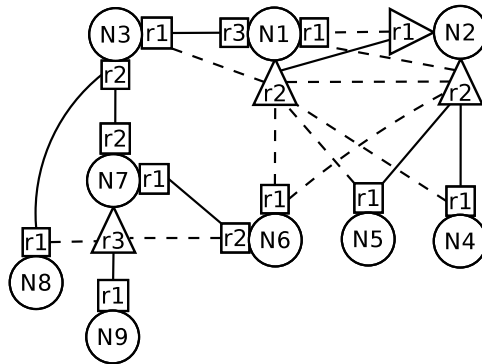


Figure 2.1: Connectivity Graph of network nodes in Fig. 1.1; routing and interference links with solid and dashed lines, respectively. Multiple radio interfaces are depicted with rectangles or triangles, corresponding to narrow beamwidth and sector directional antennas, respectively.

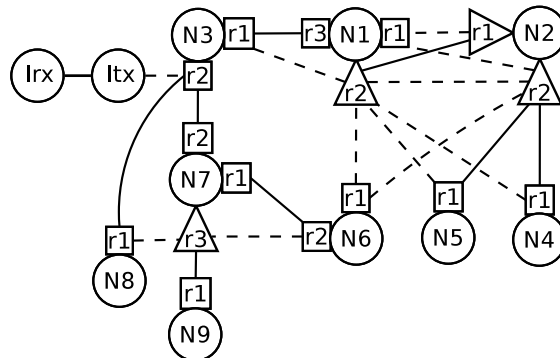


Figure 2.2: Connectivity Graph of network nodes with External Interference.



Figure 2.3: ALIX 3D2 in a waterproof case with an antenna attached to a radio interface.

In order to study the effects of possible external interference, two more nodes are added to the connectivity graph $G(V, E)$, representing an external interfering source. Fig. 2.2 shows the additional connectivity graph containing external interference for simulation purposes. Node Itx is transmitting to node Irx and it is causing interference to the interface $N_3 : r_2$ through the interference link $Itx - N_3 : r_2$. Note that the network manager does not have access to the interference nodes Itx and Irx . This means that the external interference caused by these nodes has to be detected and mitigated by the rest of the network.

The chromatic number of graph G , denoted as $\chi(G)$, is the smallest number of colors needed to color the vertices of G , so that no two adjacent vertices share the same color. The clique number of a graph G , denoted as $\omega(G)$, is the number of vertices in a maximum clique of G . Subsequently, the maximum clique of a graph G is a clique (i.e., complete subgraph) with the maximum number of vertices in G .

Connectivity between any two radio interfaces exists when the received power is above the sensitivity of the radio interface hardware. In order to serve the long-range links, the sensitivity of the receiving interfaces has to be maximized. By using the minimum possible bitrate, the sensitivity of the receivers is maximized [20]. 802.11s inherently depends on one of 802.11a, 802.11b, 802.11g or 802.11n carrying the actual traffic. The lowest bitrate of



Figure 2.4: Deployment phase.

802.11s protocol is 1Mbps and it is achieved by 802.11b PHY using DSSS (11 Chip Barker Coding) DBPSK. The sensitivity of the radio interfaces used in this work at 1Mbps is -90 dBm. There are 3 non-overlapping, orthogonal frequency channels in 802.11b (i.e., 1, 6 and 11 at 2412 MHz, 2437 MHz and 2462 MHz, respectively).

Due to the large distances in the involved wireless links along with the altitude difference of the nodes in the network, a two-ray propagation loss model is considered [21]:

$$L = \frac{\text{received power}}{\text{transmitted power}} = \begin{cases} G_T G_R \left(\frac{\lambda}{4\pi d}\right)^2, & d < d_0 \\ G_T G_R \left(\frac{h_T h_R}{d^2}\right)^2, & d \geq d_0 \end{cases} \quad (2.1)$$

where L is the one-way loss, d is the distance between transmitter and receiver, G_T and G_R are the gains of the transmitter and receiver antennas respectively, λ is the RF carrier wavelength and d_0 is given by:

$$d_0 = \frac{4\pi h_T h_R}{\lambda}$$

where h_T and h_R are the heights of the transmitter and receiver antennas, respectively. The first case of the above formula is used where $d < d_0$, i.e. free space loss, due to the placement of the antennas at high altitudes.

Each wireless node consisted of an ALIX 3D2 board which was enclosed in a waterproof case. Each board was equipped with one or more 802.11b low-cost mini PCI or USB radios. The ALIX 3D2 has two mini PCI and two USB slots, so each network node can accommodate up to four radio interfaces simultaneously (Fig. 2.3).

The establishment of reliable links with neighboring nodes, was a challenging part during the deployment phase (Fig. 2.4). The antenna alignment

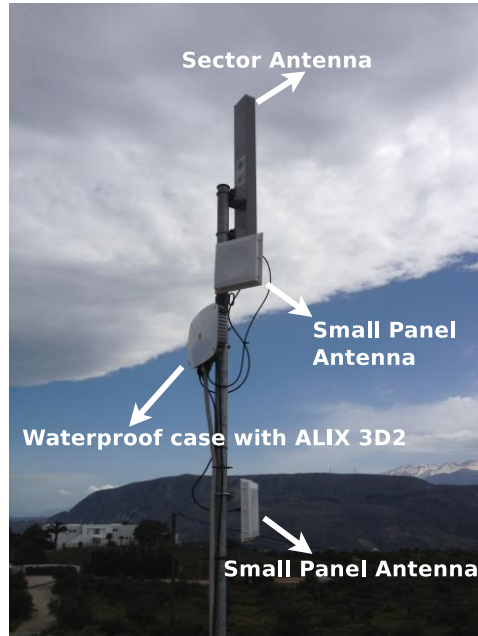


Figure 2.5: City-deployed node with multiple directive radio interfaces.

Antenna Type \ Frequency (Channel)	2412 MHz (1)	2437 MHz (6)	2462 MHz (11)
	Sector 120°	12.9634 dBi	9.7330 dBi
Sector (C) 120°	10.2863 dBi	11.5559 dBi	11.7451 dBi
Panel (Big) 60°	11.6863 dBi	13.0259 dBi	14.0251 dBi
Panel (Small) 60°	9.5863 dBi	10.5359 dBi	10.6751 dBi

Table 2.1: Antenna Gains.

was not a trivial task, due to the large distance of the network links. It was accomplished with the use of a spectrum analyzer and a frequency generator. Fig. 2.5 shows a working deployed node with the antennas aligned to its neighboring nodes.

The deployment of low cost, high-gain antennas was necessary to further increase the reception reliability. Various antennas were employed for the implementation of the network: two different broad beamwidth type antennas (120°) and two different narrow beamwidth type antennas (60°). Each one of them, has different gain in the 3 non-overlapping, orthogonal 802.11b frequency channels. It is critical to ensure for each routing link, that the

Node	Interface	Antenna Type
N_1	$N_1 : r_1$	Panel (Big)
	$N_1 : r_2$	Sector
	$N_1 : r_3$	Panel (Big)
N_2	$N_2 : r_1$	Sector (C)
	$N_2 : r_2$	Sector
N_3	$N_3 : r_1$	Panel (Big)
	$N_3 : r_2$	Panel (Big)
N_4	$N_4 : r_1$	Panel (Big)
N_5	$N_5 : r_1$	Panel (Big)
N_6	$N_6 : r_1$	Panel (Big)
	$N_6 : r_2$	Panel (Small)
N_7	$N_7 : r_1$	Panel (Small)
	$N_7 : r_2$	Panel (Big)
	$N_7 : r_3$	Sector
N_8	$N_8 : r_1$	Panel (Small)
N_9	$N_9 : r_1$	Panel (Small)

Table 2.2: Antenna Type per Radio Interface.

total transmission power (radio interface transmission power plus antenna gain) is the same among all the available frequencies. For that reason, it was necessary to perform antenna gain measurements. The various antenna gains are shown in Table 2.1. The antenna type installed at each radio interface is shown in Table 2.2. The rectangles in Fig. 2.1 represent narrow beamwidth directive antennas at the corresponding radio interfaces and the triangles represent sector directive antennas at the corresponding radio interfaces.

Chapter 3

Conflict Graph Creation & Simplification

Given the connectivity graph (Fig. 2.1) that includes the routing and interfering links among all network radio interfaces, an initial conflict graph is created [1]. In the initial conflict graph $G_c(V_c, E_c)$ (Fig. 3.1), each vertex corresponds to a *routing* link between two radio interfaces. For example, the $N_2 : r_1 - N_1 : r_2$ conflict graph vertex exists in Fig. 3.1, since $N_2 : r_1$ and $N_1 : r_2$ correspond to two different radio interfaces and there is a routing link between them. Radio interfaces of the same node operating at the same frequency channel cause leakage interference. For example, the edge between the conflict graph vertices $N_1 : r_3 - N_3 : r_1$ and $N_3 : r_2 - N_7 : r_2$, encodes the conflict due to leakage interference caused by the radio interfaces of node N_3 . Additional edges in the conflict graph encode the conflict of one link operating at the same frequency channel with other links, based on the routing and interference connectivity between the radio interfaces (Fig. 2.1).

Notation of the initial conflict graph (Fig. 3.1) is simplified by assigning numbers to each vertex. In the left graph of Fig. 3.2, vertex 1 corresponds to vertex $N_2 : r_1 - N_1 : r_2$, vertex 2 corresponds to vertex $N_1 : r_3 - N_3 : r_1$ and so forth. Thus, Fig. 3.1 and Fig. 3.2-left are equivalent.

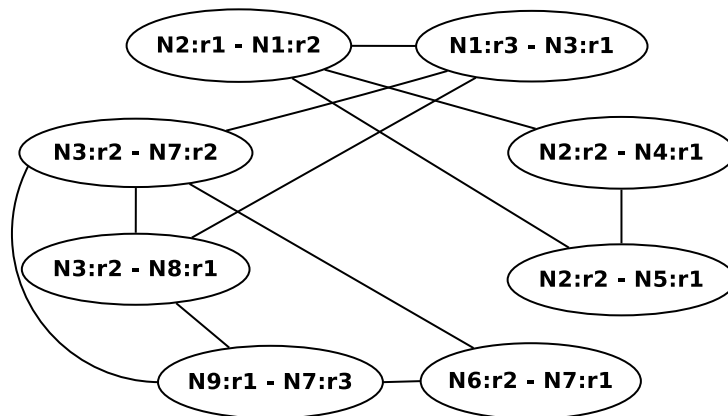


Figure 3.1: Initial Conflict Graph.

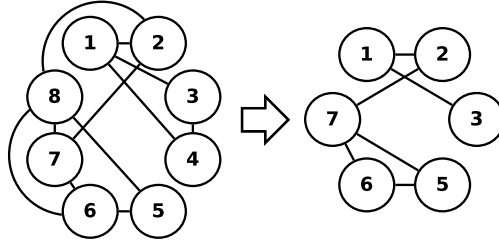


Figure 3.2: Conflict Graph before and after merging. Left graph above is equivalent to conflict graph of Fig. 3.1.

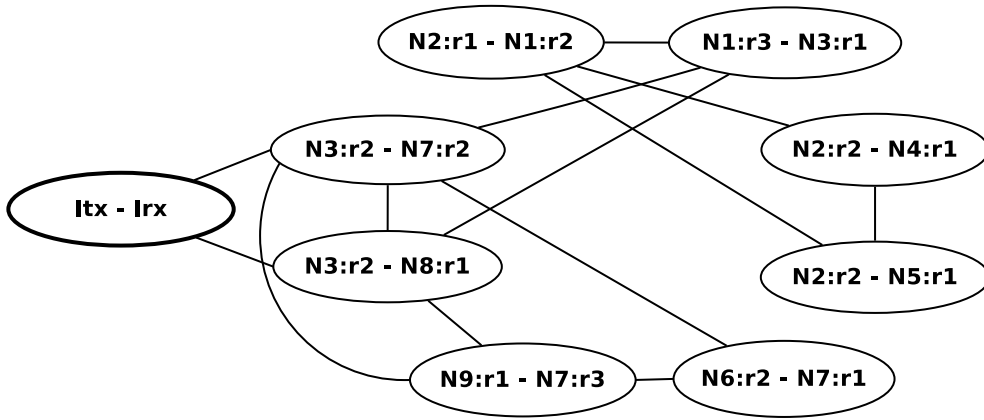


Figure 3.3: Initial Conflict Graph with External Interference.

The initial conflict graph can be further simplified, since only one color can be assigned to each radio interface and some conflict graph nodes share the same radio interface. For example, vertices 3, 4 have common radio interface $N_2 : r_2$ and vertices 7, 8 have common radio interface $N_3 : r_2$. The resulting merged vertex 3 in Fig. 3.2-right consists of radio interfaces $N_2 : r_2$, $N_4 : r_1$ and $N_5 : r_1$ and the merged vertex 7 in Fig. 3.2-right consists of radio interfaces $N_3 : r_2$, $N_7 : r_2$ and $N_8 : r_1$. The merged vertices in the modified conflict graph do not represent a link of the routing tree. Instead, they express the constraint for a common color in the subsequent graph coloring procedure.

Given the connectivity graph (Fig. 2.2) that includes the added external interference nodes, an additional conflict graph is created [1]. In the additional conflict graph (Fig. 3.3), the vertex $Itx - Irx$ corresponds to the link between the external interference nodes. The conflict of the interference link operating at the same frequency channel with the routing links that include interface $N_3 : r_2$ is encoded with additional edges between vertices $Itx - Irx$ with $N_3 : r_2 - N_7 : r_2$ and $N_3 : r_2 - N_8 : r_1$.

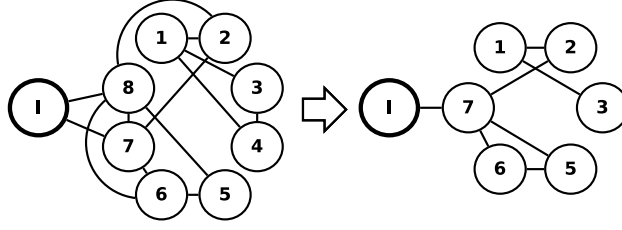


Figure 3.4: Conflict Graph before and after merging with External Interference.

The simplified notation of the connectivity graph discussed above is applied to the additional conflict graph including the external interference. The graph of Fig. 3.3 is simplified to Fig. 3.4-left. Vertex $Itx - Irx$ of Fig. 3.3 corresponds to vertex I of Fig. 3.4-left. Following the merging operation for the vertices that share a common interface, the graph of Fig. 3.4-left produces the graph of Fig. 3.4-right.

The conflict graph merging operation is formalized below and it is shown that valid coloring of the modified graph also offers valid coloring of the initial conflict graph; this finding is non-trivial, given that the two graphs describe the coloring constraints in a different way. The set of vertices in the original graph is denoted as \mathcal{U} . \mathcal{I}_0 is the set of vertices in the original conflict graph that do not need merging, while $\{\mathcal{I}_j\}_{j=1}^L$ are the *disjoint* sets of vertices in the original graph that require merging, defined through an example: in Fig. 3.2-left, set \mathcal{I}_0 consists of vertices 1, 2, 5 and 6, set \mathcal{I}_1 consists of vertices 3 and 4 and set \mathcal{I}_2 consists of vertices 7 and 8. Thus, $\mathcal{U} = \mathcal{I}_0 \cup \mathcal{I}_1 \cup \mathcal{I}_2 = \{1, 2, 3, 4, 5, 6, 7, 8\}$ and $L = 2$. Merging in the set \mathcal{I}_j , produces a new vertex i_j in the modified conflict graph. For example, the merged vertices of sets \mathcal{I}_1 , \mathcal{I}_2 , are the vertices $i_1 = 3$, $i_2 = 7$, respectively (Fig. 3.2-right). The set of conflict graph vertices after merging is denoted as $\tilde{\mathcal{U}}$. For example, $\tilde{\mathcal{U}} = \{i_1, i_2\} \cup \mathcal{I}_0 = \{1, 2, 3, 5, 6, 7\}$ in Fig. 3.2-right. $\mathcal{N}(v)$ denotes the neighboring vertices' set of vertex v and $\mathcal{C}(v)$ is the color of vertex v .

A coloring \mathcal{C} is valid for set \mathcal{U} in the initial (before merging) conflict graph when *all* the following conditions hold:

$$\mathcal{C}(v) \neq \mathcal{C}(v'), \forall v \in \mathcal{I}_0 \text{ and } \forall v' \in \mathcal{N}(v), \quad (3.1)$$

$$\mathcal{C}(v) \neq \mathcal{C}(v'), \forall v \in \mathcal{I}_j, \forall v' \in \mathcal{N}(v) \setminus \mathcal{I}_j, \forall j \in \{1, 2, \dots, L\}, \quad (3.2)$$

$$\mathcal{C}(v) = \mathcal{C}(v'), \forall v \in \mathcal{I}_j, \forall v' \in \mathcal{I}_j, \forall j \in \{1, 2, \dots, L\}. \quad (3.3)$$

Eq. (3.1) describes the constraint that neighboring vertices, which do not share a common interface in the initial conflict graph, have to be assigned

different colors. Eq. (3.2) implies that neighboring sets of vertices, which share different radio interfaces in the initial conflict graph, have to be assigned different color. Eq. (3.3) expresses the necessity of assigning the same color to vertices that share the same radio interface.

The set of vertices in the graph after merging is defined as:

$$\tilde{\mathcal{U}} = \{i_1, i_2, \dots, i_L\} \cup \mathcal{I}_0, \text{ where } i_j \in \mathcal{I}_j, \forall j \in \{1, 2, \dots, L\} \quad (3.4)$$

A coloring \mathcal{C} is valid for set $\tilde{\mathcal{U}}$ in the modified conflict graph when:

$$\mathcal{C}(v) \neq \mathcal{C}(v'), \forall v \in \tilde{\mathcal{U}} \text{ and } \forall v' \in \mathcal{N}(v). \quad (3.5)$$

Eq. (3.5) describes the constraint that neighboring vertices in the modified (merged) conflict graph, have to be assigned different colors. The following guarantees that graph coloring can be safely executed in the modified conflict graph, after merging:

Theorem 1. *Every valid coloring of \mathcal{U} is a valid coloring of $\tilde{\mathcal{U}}$ and every valid coloring of $\tilde{\mathcal{U}}$ is a valid coloring of \mathcal{U} .*

Proof. The proof is given at the Appendix. □

Chapter 4

Conflict Graph Coloring

4.1 SDP for Graph Chromatic Number Estimation

The clique number of a graph G offers a lower bound for its chromatic number, i.e., $\omega(G) \leq \chi(G)$. An example of $\omega(G) < \chi(G)$ is an odd-length cycle graph with length equal or larger than 5. Before offering any graph coloring algorithm, it is important to have a structured method to calculate the chromatic number of the graph.¹ A method based on semidefinite programming (SDP) [19] was chosen, briefly described for completeness below.

Given a graph $G = (V, E)$ on n vertices, a vector k -coloring of G is an assignment of unit vectors $\{u_i\}$ (from the \mathcal{R}^n space) to each vertex $i \in V$, such that for any two adjacent vertices i and j , the dot product of their vectors satisfies the following inequality:

$$\langle u_i, u_j \rangle \leq -\frac{1}{k-1}. \quad (4.1)$$

Given a graph $G = (V, E)$ on n vertices, a matrix k -coloring of the graph is an $n \times n$ positive semidefinite matrix $\mathbf{M} = \{m_{ij}\}$, with $m_{ii} = 1$ and $m_{ij} \leq -\frac{1}{k-1}$. The matrix and the vector k -colorings are equivalent. Thus, to solve the vector coloring, it suffices to find a matrix k -coloring. A SDP is constructed whose optimum is $-\frac{1}{k-1}$, when k is the smallest real number such that a matrix k -coloring of G exists:

$$\begin{aligned} & \text{minimize } a \\ & \text{where } \mathbf{M} = \{m_{ij}\} \text{ is positive semidefinite,} \\ & \text{subject to } m_{ij} \leq a \text{ if } (i, j) \in E, \\ & m_{ii} = 1. \end{aligned}$$

Consider a graph which has a vector (and matrix) k -coloring. This means there is a solution to the above semidefinite problem with $a = -\frac{1}{k-1}$, since every k -colorable graph has a vector k -coloring. We use this approach to find the minimum number of colors k required to successfully color a graph.

¹Useful definitions are offered in Chapter 2.

4.2 Link Protection Coloring Algorithm (LPCA)

LPCA input is a valid conflict graph $G_c(V_c, E_c)$, a set of available colors \mathcal{K} and the set of weights $\{D(i, j)\}$, between any two radio interfaces i, j , where $(i, j) \in E$ (the connectivity graph of the network). The set of weights $\{D(\cdot, \cdot)\}$ is used to decide the order with which the graph vertices are visited during algorithm execution. Higher $D(\cdot, \cdot)$ weight value means higher priority. The $D(\cdot, \cdot)$ weight of a merged vertex is defined as the maximum weight between any pair of its radio interfaces.

Set of weights $\{D(\cdot, \cdot)\}$ is also used for the case when the available colors are not enough to color the graph. In this case there will be remaining interference. LPCA will protect the links with higher weight values, while links with lower weight values will be more affected by the remaining interference.

The set of weights $\{H(\cdot, \cdot)\}$ contains information of the set of the available colors \mathcal{K} for each vertex V_c . Specifically, the weights $\{H(m, n)\}$ depend on the Packet Error Rate (PER) of each vertex $m \in V_c$ for each color $n \in \mathcal{K}$, denoted as $\text{PER}(m, n)$:

$$H(m, n) = \frac{\frac{1}{\text{PER}(m, n)}}{\sum_{1 \leq n \leq |\mathcal{K}|} \frac{1}{\text{PER}(m, n)}}, \text{ where } m \in V_c \text{ and } n \in \mathcal{K}. \quad (4.2)$$

Higher $H(m, n)$ weight value means lower internal and/or external interference, resulting in higher QoS of the frequency channel $n \in \mathcal{K}$ of vertex $m \in V_c$. The $H(m, n)$ weight of a merged vertex $m \in V_c$ is defined as the minimum $H(m, n)$ weight between the merging vertices $m \in V_c$, for each available frequency channel $n \in \mathcal{K}$. The PER statistics that are used to define the set of weights $\{H(\cdot, \cdot)\}$ are measured by FCPA, presented in the next section (Section 4.3). LPCA can be executed without the set of weights $\{H(\cdot, \cdot)\}$ and in this case they are initialized as normal random variables.

The number of available colors is denoted as $|\mathcal{K}|$. maxND is the maximum node degree of the uncolored vertices of G_c . It is noted that more than one vertices can have node degree equal to maxND . Q is a queue which includes the vertices of the conflict graph with node degree equal to maxND . LPCA visits the elements of Q by sorting them according to their weight values $D(\cdot, \cdot)$. Functions *addToQueue* and *RemoveFromQueue* are used to add and remove a vertex from Q , respectively. $\mathcal{F}(u)$ is the set of available colors that vertex u can be assigned and that set is initialized with \mathcal{K} .

In order to protect the weaker links, weight $D(i, j)$ can be initialized as $-\log(L)$, where L is the path loss in Eq. (2.1), incorporating alignment (or misalignment) of antennas, antenna gains and putting higher weight to

higher path loss. For omni-directional antennas it could be initialized as the Euclidean distance between radio interfaces i, j . Other weight definitions are possible, adhering to different QoS requirements. The neighbors of u that are already colored, have higher $D(\cdot, \cdot)$ weight values. This happens since LPCA colors the vertices with higher $D(\cdot, \cdot)$ weight values first. In the case that there is no free color for u , LPCA will assign to u the color of its neighbor with the lowest $D(\cdot, \cdot)$ weight value. In that way, the higher $D(\cdot, \cdot)$ weight valued neighbors of u are protected and the remaining interference affects the links with smaller priority (lower $D(\cdot, \cdot)$ weight values).

The $maxD$ vector is utilized; this vector is initialized as a null vector and has dimension $1 \times |\mathcal{K}|$. The indexes of $maxD$ correspond to the available colors $\{1, 2, \dots, |\mathcal{K}|\}$. This vector contains the maximum $D(\cdot, \cdot)$ weights of the neighboring vertices of u , for each available color. E.g., $maxD(3) = 10$ means that the highest $D(\cdot, \cdot)$ weighted neighbor of u at color 3 has $D(\cdot, \cdot)$ weight equal to 10. LPCA will assign to u the index of the minimum value of $maxD$. In that way, the lower $D(\cdot, \cdot)$ weighted vertices are affected by the remaining interference.

LPCA starts by finding the uncolored vertices that have the maximum node degree in the conflict graph and it inserts them into the queue Q (Lines 1-7). LPCA visits the vertices of the queue according to their $D(\cdot, \cdot)$ weight value. Higher $D(\cdot, \cdot)$ weight value vertices are visited first (Line 8). In Line 9, the $maxD$ vector is initialized with null values. In Line 10, the set of valid colors of vertex u , denoted as $\mathcal{F}(u)$, is initialized with the set of available colors \mathcal{K} . If a color c has been assigned to a neighbor of u , it is removed from the set $\mathcal{F}(u)$ of valid colors for u (Lines 11-13). In Lines 15-16 the highest $D(\cdot, \cdot)$ weight among the neighbors of u that have been assigned the color c , is stored in $maxD(c)$.

If the set $\mathcal{F}(u)$ is not an empty set, color the vertex u with the color c from set $\mathcal{F}(u)$ that has the highest $H(u, c)$ weight value (Lines 20-21). If $\mathcal{F}(u)$ is an empty set, assign to u the color c which is the index to the minimum value of $maxD$. Finally in Line 25, vertex u is removed from Q , and this process is repeated until all vertices of G_c are colored.

Algorithm 1 Link Protection Coloring Algorithm

Input: Conflict Graph $G_c(V_c, E_c)$, Set of Available Colors \mathcal{K} , Weights between Radio Interfaces $D(i, j)$, Weights of Available Colors $H(m, n)$

Output: Coloring $V_c \Rightarrow \mathcal{K}$

```

1: while  $\exists v \in V_c$  with no color assigned do
2:    $maxND = \max(deg)$  of the uncolored vertices in  $G_c$ 
3:   for  $w \in V_c$  do
4:     if  $deg(w) == maxND$  and  $w$  uncolored then
5:        $addToQueue(Q, w)$ 
6:     end if
7:   end for
8:   select  $u \in Q$  with  $\max(D(i, j))$  between radio interfaces  $i$  and  $j$  of  $u$ 
9:   initialize  $maxD(1, |\mathcal{K}|) = \bar{\mathbf{0}}$ 
10:  initialize set of free colors for  $u$ ,  $\mathcal{F}(u) = \mathcal{K}$ 
11:  for  $w \in V_c, w \neq u$  do
12:    if  $(w, u) \in E_c$  then
13:       $\mathcal{F}(u) = \mathcal{F}(u) - color(w)$ 
14:      find  $D(i, j)$  between interfaces  $i$  and  $j$  of  $w$ 
15:      if  $D(i, j) > maxD(color(w))$  then
16:         $maxD(color(w)) = D(i, j)$ 
17:      end if
18:    end if
19:  end for
20:  if  $\mathcal{F}(u) \neq \emptyset$  then
21:    assign to  $u$  the color  $c^* = \arg \max_{c \in \mathcal{F}(u)} (H(u, c))$ 
22:  else
23:    assign to  $u$  the color  $c^* = \arg \min_{c \in \mathcal{K}} (maxD(c))$ 
24:  end if
25:   $RemoveFromQueue(Q, u)$ 
26: end while

```

4.3 Frequency Channel Probing Algorithm (FCPA)

In this section a frequency channel probing algorithm for statistics collection is presented. This algorithm is used for the measurement of the overall network interference for each routing link. The output is PER statistics for each routing link on all available frequency channels. These PER statistics are used as input in LPCA, in order to detect and mitigate any possible

external interference. These statistics are used in (4.2) to produce the set of weights $\{H(\cdot, \cdot)\}$.

As input, the frequency channel probing algorithm needs the Routing Tree \mathcal{T} , the Network MAC and IP address table \mathcal{A} , the Antenna Type Set \mathcal{B} , the Primary Frequency Channel \mathcal{P} and the Set of Secondary Frequency Channels \mathcal{S} . The Routing Tree is used by the algorithm to determine the father of each child interface. The algorithm needs the Network MAC and IP addresses table to translate the MACs into IPs for the UDP transmissions that take place. Each antenna type that the network nodes use has different gains, depending on the transmission frequency channel, which are known (Table 2.1). The algorithm uses the Antenna Type Set \mathcal{B} to adjust the transmission power. The variable x is used to set the number of probe packets that are transmitted. PER is the ratio of the number of probe packets not successfully received to the number of probe packets sent (x). The Primary Frequency Channel is considered to be the main frequency channel of the link and the Secondary Frequency Channels are the frequency channels under testing. PER statistics are produced for both the Primary and the Secondary Frequency Channels.

The algorithm initially places the father interface on listening mode on primary frequency channel. The child interface randomly selects the secondary frequency channel and includes that information in the probe packets that it sends on primary frequency channel to its father interface. The child interface then changes to the secondary frequency channel. When the father interface receives the probe packets on the primary frequency channel, it calculates the PER and then switches to the secondary frequency channel based on the information that the probe packets contain.

The child interface starts the transmission of the probe packets on secondary frequency channel. When the father interface receives the probe packets on the secondary frequency channel, it calculates the PER and then both the child and the father interface switch back to the primary frequency channel. The process is then repeated.

In case the father interface does not receive any packets on primary frequency channel, the link is considered not established and no communication is available between those two interfaces.

In case that the father interface does not receive any packets on secondary frequency channel, there is a backup timer that will force the interface to switch back to the primary frequency channel before the child interface starts the next transmission.

Since the traffic follows the path from the source nodes to the gateway, the calculated PERs correspond to the links from each child interface to its father interface. Therefore PER(1,2) corresponds to the PER of child to

Algorithm 2 Frequency Channel Probing Algorithm

Input: Network Topology \mathcal{T} , Network MAC and IP Table \mathcal{A} , Antenna Type Set \mathcal{B} , Primary Frequency Channel \mathcal{P} , Set of Secondary Channels \mathcal{S} .

Output: Child-Father Link PER on Primary and Secondary Frequency Channels.

Child Interface:

- 1: Switch the Interface to Primary Frequency Channel \mathcal{P} .
 - 2: Get Father Interface t from Network Topology \mathcal{T} .
 - 3: Get MAC and IP of t from Network MAC and IP Table \mathcal{A} .
 - 4: Select Uniformly at random a Frequency Channel s from Secondary Frequency Channels set \mathcal{S} .
 - 5: Send Probe Packet $d1$ to t including s , x times.
 - 6: Switch the Interface to Frequency Channel s from step 4.
 - 7: Send Probe Packet $d2$ to t including \mathcal{P} , x times.
 - 8: Go to step 1.
-

Father Interface:

- 1: Switch the Interface to Primary Frequency Channel \mathcal{P} .
 - 2: **if** $d1$, from step 5 of Child Interface, is Received **then**
 - 3: Get the Secondary Frequency Channel s from $d1$.
 - 4: Calculate PER for the link Child to Father Interface on Primary Frequency Channel \mathcal{P} .
 - 5: Switch the Interface to Secondary Frequency Channel s .
 - 6: **if** $d2$, from step 7 of Child Interface, is Received **then**
 - 7: Get the Primary Frequency Channel P from $d2$.
 - 8: Calculate PER for the link Child to Father Interface on Secondary Frequency Channel s .
 - 9: **end if**
 - 10: **end if**
 - 11: Go to step 1.
-

father link for the color 2 of vertex 1 ($N_2 : r_1$ to $N_1 : r_2$), of the conflict graph G_c of Fig. 3.4-right.

Chapter 5

Results

5.1 Simulation Results

Throughput performance of the proposed LPCA is examined, using simulations in NS3 [22], also contrasting the results with state-of-the-art TABU coloring [6]. Network traffic monitoring is performed using Wireshark [23].

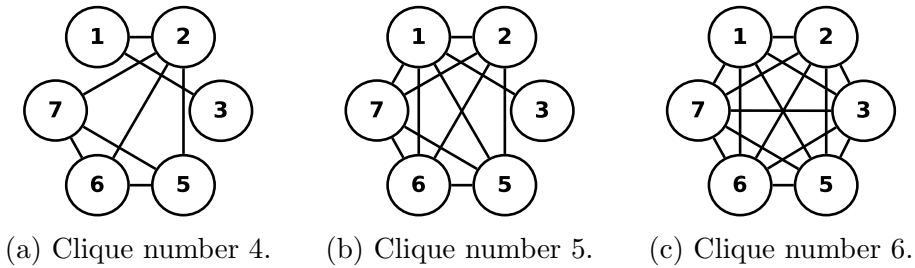


Figure 5.1: Extended Conflict Graph.

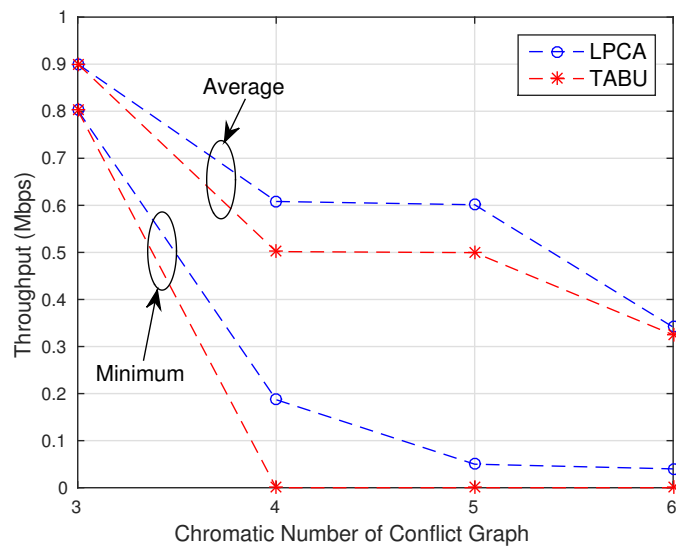


Figure 5.2: Average and Minimum Throughput of Source Nodes.

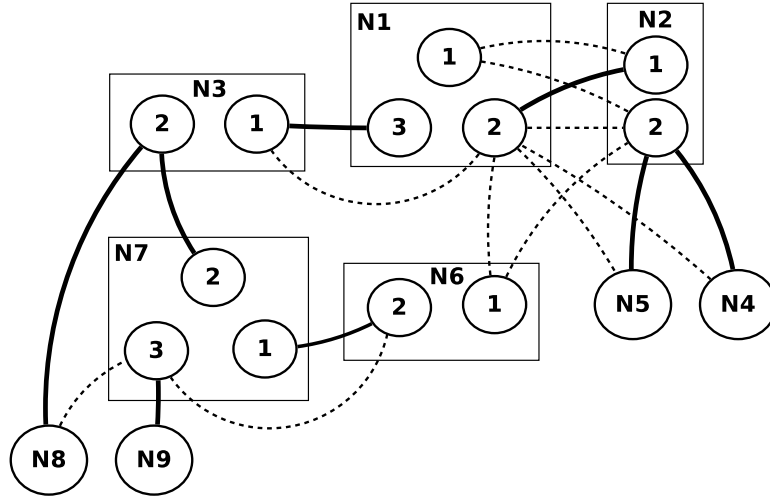


Figure 5.3: NS3 Topology of the network.

802.11s mesh nodes are assumed, operating at 1 Mbps over 802.11b at the physical/MAC and HWMP (the default 802.11s routing protocol) at the routing layer; under such assumptions, only 3 orthogonal frequency channels exist. Each node includes multiple 802.11s interfaces, with a directive antenna at each radio interface.

NS3 offers simulation tools for networks that consist of multiple omnidirectional antennas per node or single directive antennas per node in various wireless protocols; there is no current simulation tool for the combination of multiple directional antennas per node using the 802.11s/HWMP routing protocol. We approximate this setup by considering each directive radio interface as a separate *virtual* node. The virtual nodes-radio interfaces that belong to the same node are connected with links operating in “ideal” frequency channels without any propagation loss, delay or packet loss. Directivity among radio interfaces is modeled by assigning large enough loss between the virtual nodes that have no link in the connectivity graph.

The network’s setup in NS3 is shown in Fig. 5.3, where nodes N_4 , N_5 , N_6 , N_8 and N_9 are the information sources and node N_1 is the sink. The bolded links are the routing links and the rest are the interference links. The virtual nodes that model radio interfaces belonging to the same node are included into boxes, e.g. N_1 consists of nodes 1, 2 and 3 that model radio interfaces $N_1 : r_1$, $N_1 : r_2$ and $N_1 : r_3$ respectively. Nodes 1, 2 and 3 of N_1 are connected with “ideal” links.

In this section, the impact of the remaining interference (after coloring) on the average and minimum throughput is studied. Towards this goal, the connectivity graph is augmented with additional links, gradually introduc-

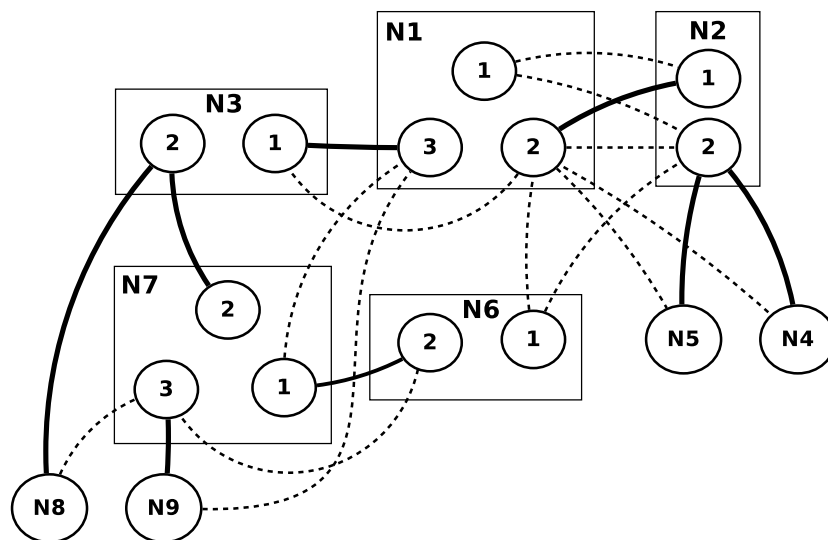


Figure 5.4: First Extended NS3 Topology.

ing more edges in the respective conflict graph; thus, the clique number is increased until the conflict graph becomes a full graph.

It is noted that the merged conflict graph in Fig. 3.2 has a max clique number of 3 and the maximal clique includes vertices 5, 6 and 7. The SDP algorithm is applied and it is found out that the minimum number of colors needed for Fig. 3.2 is 3. LPCA and TABU colorings leave no remaining interference and thus, they both achieve high average throughput, shown in Fig. 5.2 for the case of chromatic number 3. The loss of approximately 100 Kbps is due to the 802.11s/b protocol's overhead.

Two more links are introduced into the connectivity graph between radio interfaces $N_1 : r_3 - N_9 : r_1$ and $N_1 : r_3 - N_7 : r_1$. The NS3 topology and the resulting conflict graph is shown in Fig. 5.4 and Fig. 5.1a, respectively. The maximum clique number of the conflict graph has increased to 4 and this clique includes vertices 2, 5, 6 and 7. The chromatic number of that conflict graph is 4, given by the SDP algorithm. In this case, the impact of the (remaining) interference strongly depends on the coloring algorithm. The average throughput of both algorithms is severely reduced, by 292 Kbps for LPCA and by 399 Kbps for TABU algorithm, as shown in Fig. 5.2 for the case of chromatic number 4. It is noticed that LPCA achieves 10% higher throughput, as it explicitly adheres to link protection principles. Specifically, significant additional interference comes from the transmissions of radio interface $N_9 : r_1$ towards receiving radio interface $N_1 : r_3$; the latter is throughput-critical, as it serves traffic from nodes N_6 , N_8 and N_9 , through node N_3 and link $N_1 : r_3 - N_3 : r_1$.

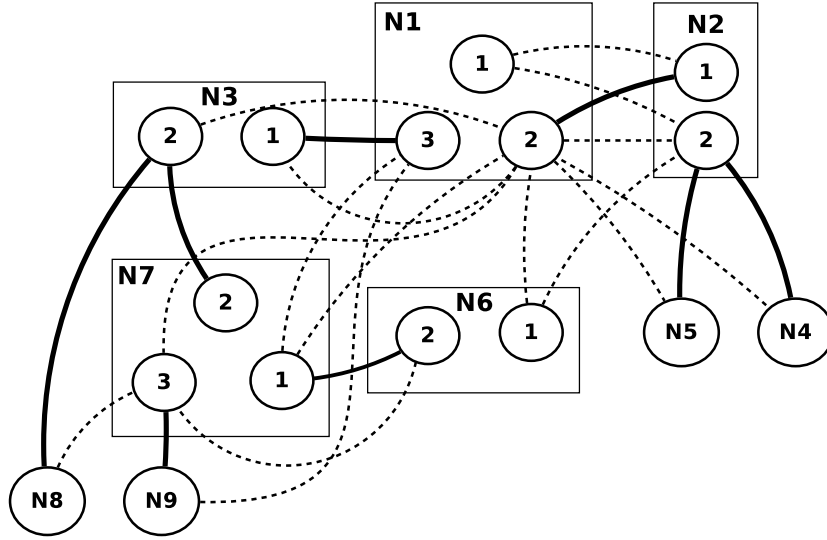


Figure 5.5: Second Extended NS3 Topology.

Three more links are added between radio interfaces $N_1 : r_2 - N_7 : r_1$, $N_1 : r_2 - N_7 : r_3$ and $N_1 : r_2 - N_3 : r_2$. The NS3 topology and the resulting conflict graph is shown in Fig. 5.5 and Fig. 5.1b, respectively. The maximum clique number of the conflict graph has increased to 5 and includes vertices 1, 2, 5, 6 and 7. The chromatic number of this graph is 5, according to the SDP algorithm. The average throughput of both algorithms is not changed significantly, as shown in Fig. 5.2 for the case of chromatic number 5. Even though that was initially surprising, it was found that the radio interfaces of the added links, mainly served as receivers for the routing paths; thus, added interference to the network was negligible. More specifically, radio interface $N_7 : r_1$ serves as receiver for radio interface $N_6 : r_2$, radio interface $N_7 : r_3$ serves as receiver for radio interface $N_9 : r_1$ and radio interface $N_3 : r_2$ serves as receiver for radio interfaces $N_8 : r_1$ and $N_7 : r_2$.

Finally, four more links are added between radio interfaces $N_2 : r_2 - N_3 : r_1$, $N_2 : r_2 - N_3 : r_2$, $N_2 : r_2 - N_7 : r_3$ and $N_2 : r_2 - N_7 : r_1$. The NS3 topology and the resulting conflict graph is shown in Fig. 5.6 and Fig. 5.1c, respectively. The max clique number has increased to 6 and it is a full graph. According to the SDP algorithm, the chromatic number of the conflict graph has increased to 6. For the case of chromatic number 6 in Fig. 5.2, a significant reduction of average throughput is observed (compared to chromatic number 5), by 260 Kbps for LPCA and by 175 Kbps for TABU. This happens because the added links introduce significant interference to the network. Specifically, the majority of added potential interference comes from radio interface $N_3 : r_1$ transmission towards receiving radio interface

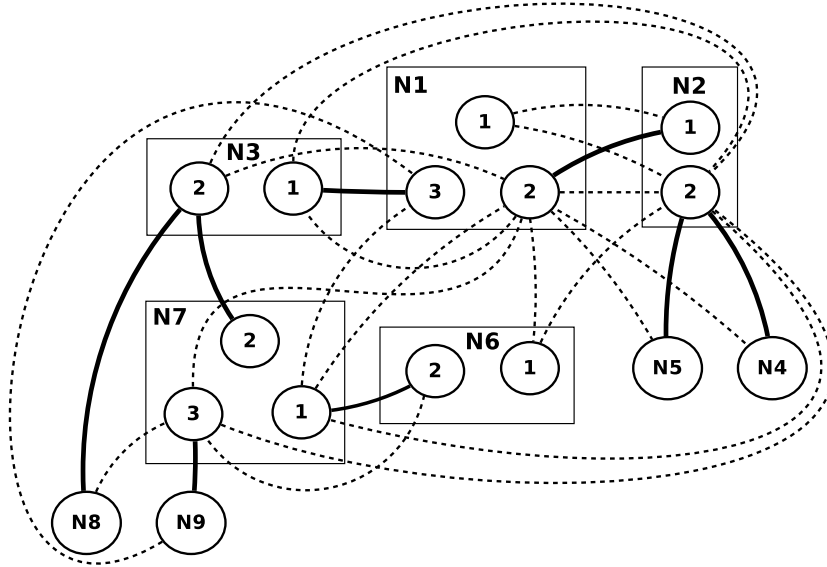


Figure 5.6: Third Extended NS3 Topology.

$N_2 : r_2$; the latter interface is critical, since it serves traffic from nodes N_4 and N_5 . In this severe interference case, LPCA achieves 2% higher average throughput.

Fig. 5.2 shows that LPCA better protects the links with higher distance by prioritizing them during the conflict graph coloring. As a result, all nodes of the network keep their connection with the rest of the network. Fig. 5.2 also shows the minimum throughput attained by the source nodes, for each case of the conflict graph's chromatic number. This is highly important, for critical, alarm-based applications, where low bit-rate information from *each* source must be able to reach the sink node. For the case of chromatic number 3, the minimum throughput achieved by a source node in the network is 800 Kbps for both algorithms. TABU algorithm achieves 0 Kbps minimum throughput for the rest of chromatic number cases. This means that there are one or more source nodes in each case that are completely cut off from the rest of the network, due to high interference. In contrast, LPCA achieves minimum throughput of 187 Kbps, 50 Kbps and 40 Kbps, for chromatic numbers 4, 5 and 6, respectively.

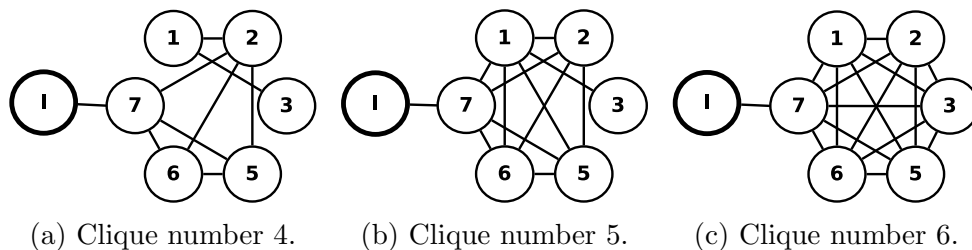


Figure 5.7: Extended Conflict Graph with External Interference.

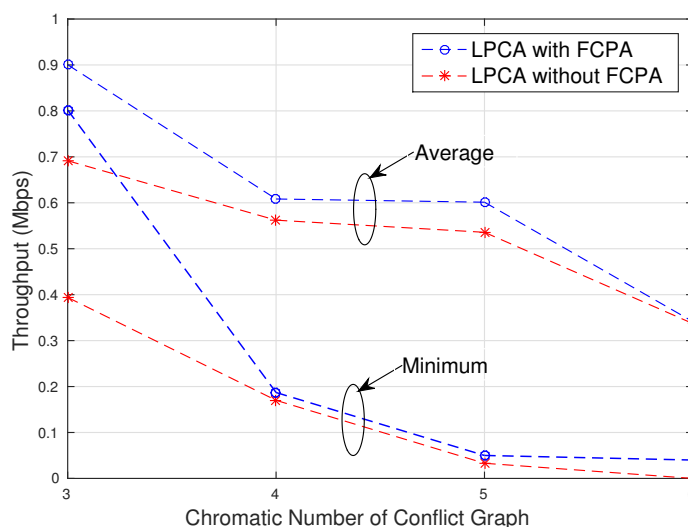


Figure 5.8: Average and Minimum Throughput Before Probing (LPCA without FCPA) and After Probing (LPCA with FCPA).

Throughput performance is also examined by utilizing the proposed probing algorithm (FCPA). For that purpose, two coloring schemes are compared. The first one is the coloring of the network by LPCA with the set of weights $\{H(\cdot, \cdot)\}$ initialized as normal random variables (LPCA without using FCPA). The second one is the coloring of the network by LPCA with the set of weights $\{H(\cdot, \cdot)\}$ produced by the PER statistics of FCPA (LPCA using FCPA).

The added external interference is modeled by an on-off traffic generator transmitting to a receiver node, noted as I_{tx} and I_{rx} in Fig. 5.9, respectively. The connectivity graph including the external interference (Fig 2.2) is also augmented with additional links, gradually increasing the clique number of the conflict graph until it becomes a full graph. The resulting augmented conflict graphs, including the external interference, are shown in Fig. 5.7.

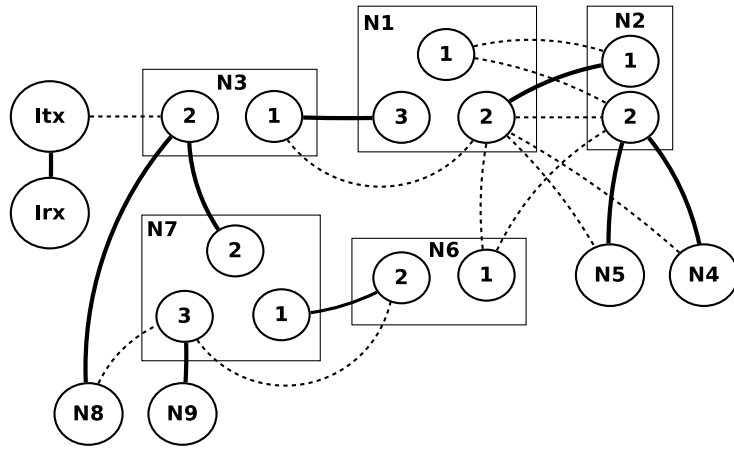


Figure 5.9: NS3 Topology of the network with External Interference.

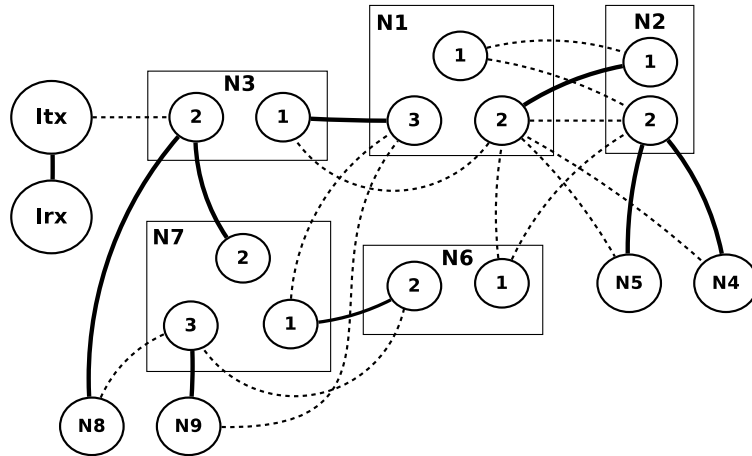


Figure 5.10: First Extended NS3 Topology with External Interference.

The NS3 topology shown in Fig. 5.10 corresponds to Fig. 5.7a, Fig. 5.11 to Fig. 5.7b and Fig. 5.12 to Fig. 5.7c respectively.

Initially, the network is colored by LPCA without using FCPA (weights $H(\cdot, \cdot)$ are set as normal random variables). External interference cannot be detected in this case. Then, FCPA performs the frequency channel scanning, detecting the external interference. This information is stored at the set of weights $\{H(\cdot, \cdot)\}$, which are used by LPCA to produce a new coloring, taking into account the external interference along with the internal interference.

The average and minimum throughput achieved with LPCA using FCPA versus LPCA without using FCPA is shown in Fig. 5.8. For the case of chromatic number 3, FCPA improves the average throughput of the network by 200Kbps and the minimum by 400Kbps. For the case of chromatic number 4,

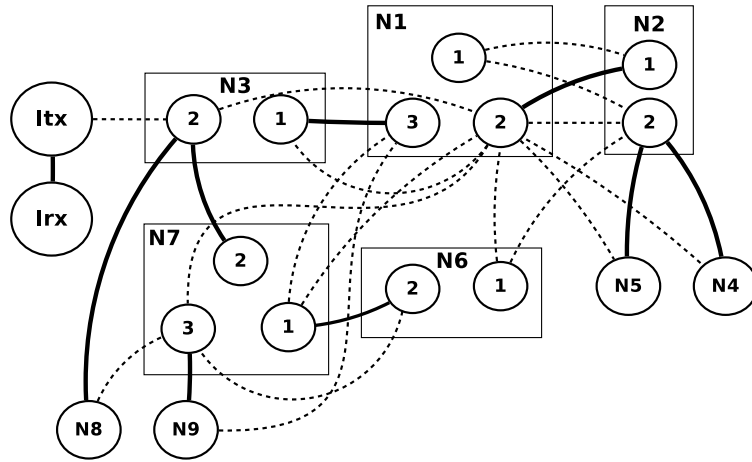


Figure 5.11: Second Extended NS3 Topology with External Interference.

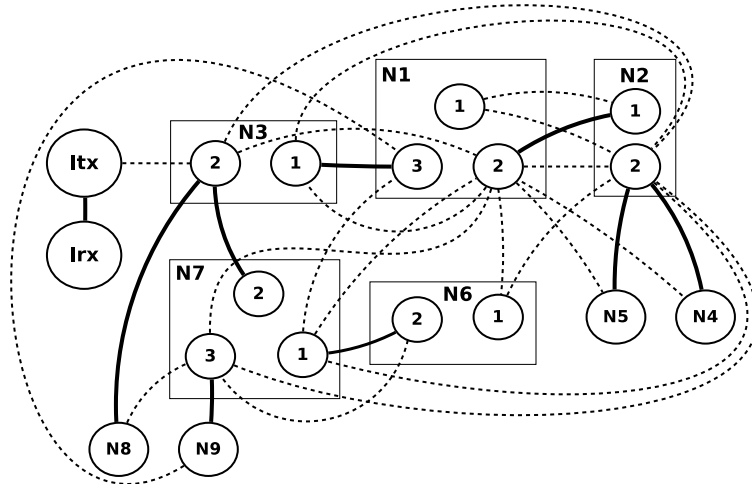


Figure 5.12: Third Extended NS3 Topology with External Interference.

the average and minimum throughput of the network is improved by 46Kbps and 17Kbps respectively. For the case of chromatic number 5, the average and minimum throughput of the network is improved by 66Kbps and 17Kbps respectively. For the case of chromatic number 6, the average and minimum throughput of the network is improved by 3Kbps and 40Kbps respectively. In the latter case the minimum throughput of LPCA without using FCPA is 0Kbps. This means that there is one or more nodes that are completely cut off from the rest of the network due to the external interference. In contrast, when FCPA is used, there are no nodes which are cut off from the network due to high external interference. This is essential for applications where information from *each* source must be able to reach the sink node.

5.2 Experimental Results

In this section, experimental results of LPCA are presented, using a city-wide rooftop testbed (Fig. 1.1). To test the efficiency of the channel assignment algorithm, two experiments were conducted. Both experiments used the routing tree of Fig. 2.1. In Case 1, all radio interfaces operated on the same frequency channel. Each node was set to transmit every two minutes twenty UDP packets towards its gateway for over 24 hours. The gateway node was able to compute the PER of the current transmission based on the number of the received packets. There were two nodes that acted as gateways, N_1 and N_3 (Table 5.1a). The PER results are shown in Table 5.1b. The displayed PER is calculated based on the whole path from each source node to the gateways.

In Case 2, LPCA was used to assign frequency channels on the radio interfaces that formed the routing tree. For this case, the coloring of LPCA was produced without the use of FCPA. This means that only the internal interference defined the coloring and that any external interference was not mitigated. Each node sent the same amount of data to its gateway and for the same duration as in Case 1. The PER results (calculated again on the whole path from the source nodes to the gateways) and the new channel assignment are shown in Table 5.1d. Table 5.1c shows the new channel assignment for the two gateway nodes.

With the exception of two nodes, the results clearly show that the channel assignment imposed by the implemented algorithm reduces the PER among the network links, offering an increased network stability. It is highly likely that the increased PER of N_2 and N_9 in Case 2, was caused by interference from other co-located 802.11 devices. There were no PER results for N_7 because this node was used only for relaying data packets between N_9 and N_3 .

Table 5.1e shows the results of FCPA that was tested on three links of the network for approximately 3 hours on each link. From these results, it is clear that the increased PER of node N_2 is caused by external interference. LPCA using randomized set of weights $\{H(\cdot, \cdot)\}$ (without using FCPA) selected the frequency channel 6 for the radio interface $N_2 : r_1$ (4% PER). The lowest PER for the link $N_2 : r_1 - N_1 : r_2$ is achieved by the frequency channel 1 (2% PER). If FCPA was used in that case, LPCA will have produced a different coloring, selecting the frequency channel 1 for the radio interface $N_2 : r_1$, reducing the PER for the specific link as a result.

Table 5.1: Experimental Results

Gateway	Interface	Channel
N_1	$N_1 : r_2$	1
	$N_1 : r_3$	1
N_3	$N_3 : r_1$	1
	$N_3 : r_2$	1

(a) Gateway Nodes for Case 1

Node	Interface	Channel	PER
N_2	$N_2 : r_1$	1	0.0004
	$N_2 : r_2$	1	
N_4	$N_4 : r_1$	1	0.538
N_5	$N_5 : r_1$	1	0.54
N_8	$N_8 : r_1$	1	0.07
N_9	$N_9 : r_1$	1	0.5
N_7	$N_7 : r_2$	1	-
	$N_7 : r_3$	1	

(b) PERs for Case 1

Gateway	Interface	Channel
N_1	$N_1 : r_2$	6
	$N_1 : r_3$	1
N_3	$N_3 : r_1$	1
	$N_3 : r_2$	11

(c) Gateway Nodes for Case 2

Node	Interface	Channel	PER
N_2	$N_2 : r_1$	6	0.01
	$N_2 : r_2$	1	
N_4	$N_4 : r_1$	1	0.41
N_5	$N_5 : r_1$	1	0.32
N_8	$N_8 : r_1$	11	0.03
N_9	$N_9 : r_1$	6	0.55
N_7	$N_7 : r_2$	11	-
	$N_7 : r_3$	6	

(d) PERs for Case 2

Child Interface	Father Interface	Channel	PER
$N_9 : r_1$	$N_7 : r_3$	1	0
		6	0
		11	0.015
$N_8 : r_1$	$N_3 : r_2$	1	0
		6	0.025
		11	0.03
$N_2 : r_1$	$N_1 : r_2$	1	0.02
		6	0.04
		11	0.12

(e) FCPA: PERs

Chapter 6

Conclusion

This work offers a frequency channel allocation policy, targeting resource constrained, *city-wide* rooftop deployments. Variable number of 802.11s (mesh) radio interfaces and different kinds of directivity antennas were employed, across the various network nodes. Results shown that nodes in resource constrained networks, depending on sensitive links, often encounter connectivity loss issues due to heavy interference (internal and/or external). The proposed frequency channel allocation policy mitigates this phenomenon, by protecting the weaker links using network planner-defined weights. Additionally, it offers better results in terms of average and minimum (worst-case) throughput, compared to non-link protection methodologies. Such QoS improvement may be deemed critical in practice. A merging technique of the vertices that share a common interface is also presented. SDP is used in the merged conflict graph to approximate the chromatic number of the graph. Finally, a modification of NS3 is offered in order to accommodate multiple radio interfaces per node, using directional antennas in 802.11s networks.

It would be interesting to investigate the scalability of the proposed algorithms. Additionally, the implementation of a distributed approach for the frequency channel allocation problem, is left for future work.

Appendix A

Proof of Theorem 1

Proof. Choose a valid coloring \mathcal{C} of \mathcal{U} . Create $\tilde{\mathcal{U}}$ as in (3.4). Since (3.1) holds, it follows that $\mathcal{C}(v) \neq \mathcal{C}(v')$, $\forall v \in \mathcal{I}_0$ and $\forall v' \in \mathcal{N}(v)$. Functions g , g^{-1} are defined as follows:

$$g_j(v) = i_j, \forall v \in \mathcal{I}_j, \forall j \in \{1, 2, \dots, L\}. \quad (\text{A.1})$$

$$g_j^{-1}(i_j) = j, \forall j \in \{1, 2, \dots, L\}. \quad (\text{A.2})$$

Eq. (A.1) returns the merged vertex i_j of the set \mathcal{I}_j . Eq. (A.2) returns the unique index j to the original set \mathcal{I}_j of the merged vertex i_j . From Eq. (A.1), $\forall v \in \mathcal{I}_j, \forall v' \in \mathcal{I}_j$ and $\forall j \in \{1, 2, \dots, L\}$ it follows that $g_j(v) = g_j(v') = i_j$ and thus,

$$\mathcal{C}(i_j) = \mathcal{C}(v) = \mathcal{C}(v'). \quad (\text{A.3})$$

From Eq. (A.2), $\forall v \in \mathcal{I}_0, \forall v' \in \mathcal{N}(v) \cap \tilde{\mathcal{U}} \cap \mathcal{I}_j, \forall v'' \in (\mathcal{N}(v) \setminus \tilde{\mathcal{U}}) \cap \mathcal{I}_j, \forall j \in \{1, 2, \dots, L\}$ it is obtained that $v' \in \mathcal{I}_{g^{-1}(i_j)=j}$ and $v'' \in \mathcal{I}_{g^{-1}(i_j)=j}$ and hence,

$$g_j(v'') = g_j(v') = i_j. \quad (\text{A.4})$$

Note that $v' = i_j$ but $v'' \neq i_j$. From Eq. (3.3),

$$\mathcal{C}(v') = \mathcal{C}(i_j) = \mathcal{C}(v''). \quad (\text{A.5})$$

From Eq. (3.1),

$$\mathcal{C}(v) \neq \mathcal{C}(v') = \mathcal{C}(i_j) = \mathcal{C}(v''). \quad (\text{A.6})$$

From Eq. (A.1), $\forall v \in \mathcal{I}_j, \forall v' \in \mathcal{N}(v) \cap \mathcal{I}_{j'} \subseteq (\mathcal{N}(v) \setminus \mathcal{I}_j), \forall j' \neq j$, where $j, j' \in \{1, 2, \dots, L\}$ it follows that

$$g_j(v) = i_j \neq i_{j'} = g_{j'}(v'). \quad (\text{A.7})$$

From Eq. (3.2),

$$\mathcal{C}(v) = \mathcal{C}(i_j) \neq \mathcal{C}(i_{j'}) = \mathcal{C}(v'). \quad (\text{A.8})$$

From Eqs. (A.3)-(A.8), it follows that \mathcal{C} is a valid coloring of $\tilde{\mathcal{U}}$ (i.e. Eq. (3.5) holds).

For the converse, choose a valid coloring $\hat{\mathcal{C}}$ of $\tilde{\mathcal{U}}$. Due to Eq. (3.5) it follows that

$$\hat{\mathcal{C}}(v) \neq \hat{\mathcal{C}}(v'), \forall v \in \mathcal{I}_0 \subseteq \tilde{\mathcal{U}} \text{ and } \forall v' \in \mathcal{N}(v). \quad (\text{A.9})$$

Using Eq. (A.2),

$$\hat{\mathcal{C}}(v) = \hat{\mathcal{C}}(v'), \forall v \in \mathcal{I}_j, \forall v' \in \mathcal{I}_j, j \in \{1, 2, \dots, L\}. \quad (\text{A.10})$$

From Eq. (A.1), $\forall v \in \mathcal{I}_j \cap \tilde{\mathcal{U}}, \forall v' \in \mathcal{N}(v) \cap \mathcal{I}_{j'} \cap \tilde{\mathcal{U}}, \forall j' \neq j$, with $j, j' \in \{1, 2, \dots, L\}$ it follows that $\hat{\mathcal{C}}(g_j(v) = i_j) \neq \hat{\mathcal{C}}(g_{j'}(v') = i_{j'})$. Eq. (A.2) results to

$$\hat{\mathcal{C}}(\mathcal{I}_{g^{-1}(i_j)=j}) \neq \hat{\mathcal{C}}(\mathcal{I}_{g^{-1}(i_{j'})=j'}). \quad (\text{A.11})$$

From Eqs. (A.9)-(A.11), it follows that $\hat{\mathcal{C}}$ is a valid coloring of \mathcal{U} , i.e. Eqs. (3.1)-(3.3) hold and the proof is completed. \square

Bibliography

- [1] D. Ntilis, P. Oikonomakos, V. Papadakis, A. Inglezakis, A. G. Dimitriou, and A. Bletsas, “Frequency planning for a multi-radio 802.11s city-wide water management network,” in *Proc. of the 1st ACM Int. Workshop on Cyber-Physical Systems for Smart Water Networks*, Seattle, WA, USA, Apr. 2015, pp. 6:1–6:6.
- [2] A. G. Dimitriou, D. Ntilis, P. Oikonomakos, A. Inglezakis, V. Papadakis, and A. Bletsas, “Designing limited-EIRP, long-distance links for water management networks using polarization diversity and redundant routing paths,” in *Proc. of the 1st ACM Int. Workshop on Cyber-Physical Systems for Smart Water Networks*, Seattle, WA, USA, Apr. 2015, pp. 4:1–4:5.
- [3] V. Angelakis, S. Papadakis, N. Kossifidis, V. A. Siris, and A. Traganitis, “The effect of using directional antennas on adjacent channel interference in 802.11a: Modeling and experience with an outdoors testbed,” in *Int. Symp. on Modeling and Optim. in Mobile, Ad Hoc, and Wireless Networks and Workshops (WiOPT)*, Berlin, Germany, Mar. 2008.
- [4] T. Staub, M. Anw, K. Baumann, T. Braun, M. Brogle, K. Dolfus, C. Flix, and P. K. Goode, “Connecting remote sites to the wired backbone by wireless mesh access networks,” in *European Wireless Conf. (EW)*, Lucca, Italy, Apr. 2010.
- [5] W. Klotz, “Graph coloring algorithms,” *Mathematics Report*, vol. 5, no. 2002, pp. 1–9, 2002.
- [6] A. P. Subramanian, H. Gupta, S. R. Das, and J. Cao, “Minimum interference channel assignment in multiradio wireless mesh networks,” *IEEE Trans. Mobile Comput.*, vol. 7, no. 12, pp. 1459–1473, Dec. 2008.
- [7] A. Hertz and D. de Werra, “Using Tabu search techniques for graph coloring,” *Computing*, vol. 39, no. 4, pp. 345–351, 1987.

-
- [8] S. Yuan, S. Varma, and J. P. Jue, “Minimum-color path problems for reliability in mesh networks,” in *Proc. IEEE Int. Conf. on Computer Commun. (INFOCOM)*, Miami, FL, USA, Mar. 2005, pp. 2658–2669.
- [9] O. Bazan and M. Jaseemuddin, “A conflict analysis framework for QoS-aware routing in contention-based wireless mesh networks with beam-forming antennas,” *IEEE Trans. Wireless Commun.*, vol. 10, no. 10, pp. 3267–3277, Oct. 2011.
- [10] G. R. Hiertz, D. Denteneer, S. Max, R. Taori, J. Cardona, L. Berlemann, and B. Walke, “IEEE 802.11s: The WLAN Mesh Standard,” *IEEE Trans. Wireless Commun.*, vol. 17, no. 1, pp. 104–111, Feb. 2010.
- [11] S. M. S. Bari, F. Anwar, and M. H. Masud, “Performance study of hybrid wireless mesh protocol (HWMP) for IEEE 802.11s WLAN mesh networks,” in *Proc. IEEE Int. Conf. on Computers and Commun. Engineering (ICCCE)*, Kuala Lumpur, Malaysia, Jul. 2012, pp. 712–716.
- [12] W. Wong and S.-H. G. Chan, “Topology optimization for wireless mesh with directional antennas,” in *Proc. IEEE Int. Conf. on Commun. (ICC)*, Sydney, Australia, Jun. 2014, pp. 2791–2796.
- [13] D. S. J. De Couto, D. Aguayo, J. Bicket, and R. Morris, “A high-throughput path metric for multi-hop wireless routing,” in *Proc. ACM Int. Conf. on Mobile Computing and Networking (MOBICOM)*, San Diego, CA, USA, Sep. 2003, pp. 134–146.
- [14] S. Biswas and R. Morris, “Exor: Opportunistic multi-hop routing for wireless networks,” in *Proc. ACM SIGCOMM*, Philadelphia, PA, USA, Aug. 2005, pp. 133–144.
- [15] A. Raniwala and T. Chiueh, “Architecture and algorithms for an IEEE 802.11-based multi-channel wireless mesh network,” in *Proc. IEEE Int. Conf. on Computer Commun. (INFOCOM)*, Miami, FL, USA, Mar. 2005, pp. 2223–2234.
- [16] G. Athanasiou, I. Broustis, T. Korakis, and L. Tassiulas, “Routing-aware channel selection in multi-radio mesh networks,” in *Proc. IEEE Int. Conf. on Commun. (ICC)*, Dresden, Germany, Jun. 2009, pp. 1–6.
- [17] M. Alicherry, R. Bhatia, and L. E. Li, “Joint channel assignment and routing for throughput optimization in multi-radio wireless mesh networks,” in *Proc. ACM Int. Conf. on Mobile Computing and Networking (MOBICOM)*, Cologne, Germany, Aug. 2005, pp. 58–72.

-
- [18] S. Avallone, I. F. Akyildiz, and G. Ventre, “A channel and rate assignment algorithm and a layer-2.5 forwarding paradigm for multi-radio wireless mesh networks,” *IEEE/ACM Trans. Netw.*, vol. 17, no. 1, pp. 267–280, Feb. 2009.
- [19] D. Karger, R. Motwani, and M. Sudan, “Approximate graph coloring by semidefinite programming,” *Journal ACM*, vol. 45, no. 2, pp. 246–265, Mar. 1998.
- [20] B. Razavi, *RF Microelectronics*. New Jersey: Prentice-Hall, 1998.
- [21] W. C. Jakes and D. C. Cox, Eds., *Microwave Mobile Communications*. Wiley-IEEE Press, 1994.
- [22] “NS3,” <https://www.nsnam.org/>.
- [23] “Wireshark,” <https://www.wireshark.org/>.